MATERIALS PHYSICS AND MECHANICS RESEARCH ARTICLE

Submitted: November 11, 2025 **Revised: December 2, 2025** **Accepted: December 10, 2025**

The influence of microplastic deformation on the performance of a shape memory alloy vibration protection system: a modeling study

F.S. Belyaev [1] ✉, A.E. Volkov [2], M.E. Evard [2], M.S. Starodubova [2]

[1] Institute for Problems of Mechanical Engineering RAS, St. Petersburg, Russia

[2] St. Petersburg State University, St. Petersburg, Russia

✉ belyaev_fs@mail.ru

ABSTRACT

Shape memory alloys are promising for vibration protection systems but their long-term performance is challenged by functional fatigue due to microplastic deformation. A previously developed microstructural model that explicitly accounts for the evolution of microplastic deformation is utilized in the research to investigate the influence of this phenomenon. A one-dimensional oscillatory system with a payload isolated by two TiNi alloy springs is investigated. Numerical simulations compare the device's response in austenitic and martensitic states, with and without microplasticity, under harmonic excitation. The results confirm that microplastic deformation significantly alters the dynamic characteristics of the system, highlighting the necessity of its inclusion for accurate performance prediction. Furthermore, the analysis demonstrates the superior performance of the shape memory alloy system compared to linear elastic counterparts, showing its inherent ability to mitigate resonance across a frequency range.

KEYWORDS

shape memory alloys • vibration protection • microplastic deformation • microstructural modeling

Acknowledgements. *The research was carried out within the state assignment of Ministry of Science and Higher Education of the Russian Federation (theme No. 124041500009-8).*

Citation: Belyaev FS, Volkov AE, Evard ME, Starodubova MS. The influence of microplastic deformation on the performance of a shape memory alloy vibration protection system: a modeling study. *Materials Physics and Mechanics.* 2026;54(1): 42–56.
http://dx.doi.org/10.18149/MPM.5412026_6

Introduction

Shape memory alloys (SMAs) represent a class of functional materials that hold a key position in solving complex engineering problems due to their unique properties. These primarily include the shape memory effect (the ability to recover significant strain upon heating) and pseudoelasticity (superelasticity) – the recovery of strain upon unloading. These macroscopic phenomena are caused by a thermoelastic martensitic transformation and accompanying processes: martensite reorientation (manifested as pseudo-plasticity) and the movement of phase and twin boundaries. Thanks to this, SMAs enable the creation of mechanical devices such as dampers, isolators, and actuators, which often surpass traditional counterparts in functionality and reliability [1–5].

The relevance of SMA application in the construction industry is particularly high for tasks of seismic protection and vibration isolation. Widely used passive damping devices – rubber-metal bearings, friction dampers, and viscoelastic dampers – have a number of fundamental limitations [6,7]. Rubber isolators are characterized by issues of aging, sensitivity to temperature fluctuations, and significant residual deformations after

strong disturbances. Friction devices require regular maintenance and can lose reliability in the long term, while many types of metallic dampers are susceptible to low-cycle fatigue and require replacement after activation. The implementation of SMAs in damping and isolating systems allows for overcoming these drawbacks, offering a path towards creating resilient and self-centering structures [2–5,8–13].

The following SMA properties are key for application in vibration protection:

1. High damping capacity associated with hysteresis during phase transformations and martensite reorientation. Energy dissipation occurs both in the high-temperature austenitic state due to direct stress-induced martensitic transformation (requiring energy for crystal lattice rearrangement) and in the low-temperature martensitic state due to irreversible movement of twin boundaries. For TiNi-based alloys, this effect has been previously studied in detail [14] and continues to be investigated in new compositions [15,16].
2. Self-centering nature provided by the shape memory effect. This property allows a structure to return to its original position after a seismic event, minimizing residual deformations, which is critically important for maintaining the building's functionality [17–21].
3. High fatigue strength under large strains (up to 6–8 %), which is due to the predominance of reversible martensitic transformation over irreversible dislocation slip. This makes SMAs ideal candidates for cyclically loaded elements in seismic isolation [22–24].

The evolution of SMA-based device designs began with relatively simple forms. Early developments widely used wire elements, which demonstrated high fatigue strength and effective energy dissipation. Cyclic tensile experiments confirmed that such devices dissipate energy stably, and the accumulation of residual deformation slows down with an increasing number of cycles [25]. Their potential for use as hysteretic dampers in braces and column bases remains high. Subsequently, the range of configurations expanded. For example, SMA dampers in the form of rings [26], curved plates [27], helical springs [28], washers [20,28], and ring springs [29] were proposed, which demonstrated high load-bearing capacity and potential for use as passive vibration isolators in various industries. Modern research is focused on creating more complex structures, such as SMA-based composites [30–32] and porous SMA structures [33].

One of the most promising directions is the development of adaptive and tunable vibration protection systems. The ability to control the phase state (and, consequently, the stiffness and damping) of an SMA working element through thermal activation paves the way for smart systems. A classic problem of passive inertial dampers is their tuning to a fixed frequency, whereas the natural frequency of a structure can change (for example, due to changes in mass, nonlinear behavior during strong earthquakes, or traffic movement on a bridge). Research, such as that in [34,35], has confirmed the possibility of retuning the frequency of an inertial damper with SMA elements. Studies [36,37] have proposed controlled vibration damping systems based on SMA composites.

Since SMAs are characterized by a nonlinear stress-strain relationship, as well as a strong dependence of their properties on temperature and loading history, reliable means of modeling their mechanical behavior are required for the successful design of vibration protection devices. However, most works on this topic are experimental, and in those where modeling was performed, the simplest phenomenological SMA models were used, allowing only for some quantitative estimates of the device response [18,35,38,39]. Exceptions are the works [40,41], which modeled vibration protection devices with helical

and slotted springs made of TiNi alloy. A microstructural model [42] capable of describing all the main SMA effects was used to describe the mechanical behavior of the working elements. Thanks to the high predictive power of this model, it was possible to obtain a good estimate of the performance of the vibration protection devices under different phase states of the working elements.

However, one of the main problems limiting the predictability of the long-term behavior of SMAs is the instability of their functional properties under cyclic loading. Since martensitic transformations involve a crystal lattice transformation, the growth of a new phase crystal within the austenitic matrix is accompanied by significant interfacial stresses. This leads to the accumulation of irreversible microplastic deformation (MPD) in the boundary regions, caused by the generation and movement of dislocations [43,44]. This phenomenon has a dual influence on performance characteristics:

1. On the one hand, MPD causes irreversible shape changes and the generation of structural defects, which in the long term accelerate fatigue failure. Furthermore, these accumulated changes distort the kinetics of subsequent martensitic transformations, leading to the degradation of functional properties — a shift in characteristic stresses and temperatures, and a reduction in the hysteresis loop and the shape memory effect.
2. On the other hand, since the generation and movement of dislocations require energy, MPD is an additional mechanism of energy dissipation, which theoretically can increase the damping capacity of the material, especially in the initial stages of cyclic loading.

Thus, the influence of MPD on the vibration protection properties of SMAs is complex and ambiguous. However, even in studies [40,41], when describing vibration protection systems, the contribution of microplasticity to the total strain was considered insignificant and was neglected. Nevertheless, it remains unclear how justified this approach is from the perspective of assessing damping properties.

In view of the above, it can be assumed that MPD significantly affects the performance of SMA-based vibration protection devices. Ignoring it in mechanical models may lead to significant errors in predicting damping characteristics and long-term stability. In this regard, the aim of this work is a systematic investigation of the influence of MPD on the effectiveness of vibration protection devices. To achieve this aim, an improved microstructural model that takes this mechanism into account will be used. Based on this model, a parametric study of an oscillatory system will be conducted to quantitatively assess the contribution of microplasticity to energy dissipation and the change in the dynamic response of the structure as a whole.

Materials and Methods

Methodology for modeling of the SMA mechanical behavior

To describe the complex mechanical behavior of SMAs in this work a microstructural model previously developed by the authors [45–50] is used. This approach allows for the correct accounting of the main deformation mechanisms characteristic of SMAs, including MPD. This model and some of its variations have proven themselves to be effective in describing such phenomena in SMA as: fatigue fracture [45], plastic deformation [46], deformation during isothermal holding [47], the effect of martensite stabilization [48], loading under conditions of heat exchange with the environment [49], and the operation of an SMA

specimen under conditions of a thermomechanical drive [50]. Therefore, it can be said that the proposed model has great predictive power and can be applied to solving engineering problems, in particular for modeling vibration protection devices based on SMA.

Basic model principles

The model describes the behavior of a representative volume of material, which is considered as a material point. The key principle lies in the multi-level description of the microstructure. The representative volume consists of numerous grains with different crystallographic orientations. Each grain, in turn, can contain austenite and/or several orientational variants of martensite.

According to the Reuss hypothesis, the macroscopic strain of the representative volume ε is calculated as the average over all orientations ω of the strains of individual grains $\varepsilon^{gr}(\omega)$:

$$\varepsilon = \sum_{\omega} f(\omega)\varepsilon^{gr}(\omega), \quad (1)$$

where $f(\omega)$ is the volume fraction of grains with orientation ω.

Kinematics of deformation at the grain level

The strain of an individual grain is represented as the sum of contributions from various physical mechanisms:

$$\varepsilon^{gr} = \varepsilon^{E} + \varepsilon^{T} + \varepsilon^{Ph} + \varepsilon^{MP}, \quad (2)$$

where ε^{E} is elastic strain (according to Hooke's law), ε^{T} is thermal strain (due to thermal expansion), ε^{Ph} is phase strain (associated with the martensitic transformation), ε^{MP} is microplastic strain (associated with plastic accommodation of martensite).

Description of phase transformation

To describe the phase strain, internal variables Φ_n are introduced, where $\frac{\Phi_n}{N}$ represents the volume fraction of the *n*-th orientational variant of martensite (*N* is the total number of variants). The phase strain of a grain is calculated as the averaged contribution of all martensite variants:

$$\varepsilon^{Ph} = \frac{1}{N}\sum_{n=1}^{N} \Phi_n D^n, \quad (3)$$

where D^n is the Bain strain tensor for the *n*-th martensite variant.

The condition determining the onset and course of martensitic transformation is formulated through the balance of thermodynamic forces:

$$F_n = \pm F^{fr}, \quad (4)$$

where F_n is the generalized thermodynamic force causing the growth of the *n*-th variant of martensite, F^{fr} is the dissipative force that prevents the movement of interphase boundaries and causes the presence of temperature-phase hysteresis, the "+" sign corresponds to the forward transformation (austenite → martensite), and the "−" sign to the reverse transformation (martensite → austenite).

The thermodynamic forces F_n and F^{fr} are calculated as follows:

$$F_n = \frac{q_0}{T_0}(T - T_0) + \sigma_{ij} : D_{ij}^n - \mu \sum_{m=1}^{N} A_{mn} (\Phi_m - b_m), \quad (5)$$

$$F^{fr} = q_0 \frac{M_s - T_0}{T_0}, \quad (6)$$

where q_0 is the latent heat of transformation, T_0 is the temperature of thermodynamic phase equilibrium (austenite and martensite), T is the temperature of representative

volume, σ is applied stress, b is the density of oriented defects, A is the matrix that determines the interaction of martensite variants described in detail in [51,52], M_s is the start temperature of the forward martensitic transformation.

The coefficient μ and the equilibrium temperature T_0 depend on the material constants and can be calculated as follows:

$$\mu = -\frac{q_0(M_s - M_f)}{T_0(1-2\alpha)}, \quad (7)$$

$$T_0 = \frac{M_s + A_f}{2}, \quad (8)$$

where M_f and A_f are the finish temperatures of the forward and reverse martensitic transformations respectively, α is a material constant characterizing the coherency of martensitic phases.

Accounting for microplastic deformation

The accumulation of MPD is a direct consequence of martensitic transformation. Transformation incompatibility between the growing martensite crystals and the surrounding austenite matrix, arising from differences in crystal lattices, generates significant localized internal stresses. To relax these stresses, accommodative microplastic flow occurs in the boundary regions. Although this flow is initially localized, its contribution can manifest itself at the macroscopic level during the formation of oriented martensite. In this case, the most favorably oriented martensite variants predominate, their volume fraction increasing. Since the MPD associated with the growth of a particular variant is consistent with its Bain strain, this leads to the summation of unidirectional microshears. As a result, the irreversible strain, initially dispersed in microvolumes, accumulates, contributing to the overall macroscopic deformation of the material. A key assumption in describing this deformation mechanism is that the MPD associated with the growth of a particular martensite variant is proportional to its Bain strain deviator:

$$\varepsilon^{MP} = \frac{1}{N}\sum_{n=1}^{N} \kappa \varepsilon_n^{mp} dev(D^n), \quad (9)$$

where ε_n^{mp} is the measure of MPD associated with the growth of the *n*-th martensite variant, κ is the scaling coefficient.

The conditions for the onset of microplastic flow are similar to the condition of plastic flow in the one-dimensional case, taking into account kinematic (translational) and isotropic hardening, where the role of stress is played by the generalized thermodynamic force F_n^p, and the kinematic and isotropic hardening correspond to the thermodynamic forces F^y and F_n^ρ:

$$\left|F_n^p - F_n^\rho\right| = F^y, \quad \left(F_n^p - F_n^\rho\right) dF_n^p > 0. \quad (10)$$

The generalized thermodynamic force causing MPD is calculated as follows:

$$F_n^p = \mu \sum_{m=1}^{N} A_{mn}(\Phi_m - b_m). \quad (11)$$

Evolution of defects and hardening

Microplastic flow is accompanied by the accumulation of two types of defects: *oriented defects* b, that create oriented long-range stress fields, and *scattered defects* f distributed in the volume. The evolution of defect densities is described by the equations:

$$\dot{b_n} = \dot{\varepsilon}_n^{mp} - \frac{1}{\beta^*}|b_n|\dot{\varepsilon}_n^{mp} H\left(b_n \dot{\varepsilon}_n^{mp}\right), \quad (12)$$

$$\dot{f} = \sum_{m=1}^{N} |\dot{\varepsilon}_m^{mp}| + r_1(f - f_0)\Phi^{gr}H(-\Phi^{gr}), \quad (13)$$

where H is the Heaviside function, β^* is the maximum density of oriented defects, r_1 is the recovery coefficient, f_0 is the equilibrium density of scattered defects, Φ^{gr} is volume fraction of all martensite variants in grain.

To obtain a closed system of equations, it is necessary to introduce hardening laws. The model assumes that scattered defects impede dislocation movement, thereby increasing the yield stress. Consequently, their density is related to isotropic hardening. Clusters of oriented defects create internal stress fields, the effect of which is combined with external stress, shifting the center of the yield surface. Consequently, their density is related to kinematic hardening. Linear dependencies are proposed to relate hardening to defect densities:

$$F_n^{\rho} = a_{\rho} b_n, \quad (14)$$

$$F^{y} = a_y f, \quad (15)$$

where a_{ρ} and a_y are material constants determining the intensity of the corresponding type of hardening.

Equations (4), (10), (12)–(15) form a closed system that allows for calculating the evolution of all internal variables. Formulas (1)–(3) and (9) are used to calculate material deformations under thermomechanical loading, which is necessary for the subsequent analysis of vibration protection devices.

Model of vibration protection device

This paper presents a numerical study of the effectiveness of a vibration isolation device, the schematic of which is shown in Fig. 1. The device consists of a rigid housing within which a payload is suspended by two helical springs made of TiNi alloy. The springs, which serve as the working elements, are designed to isolate the payload from external vibration.

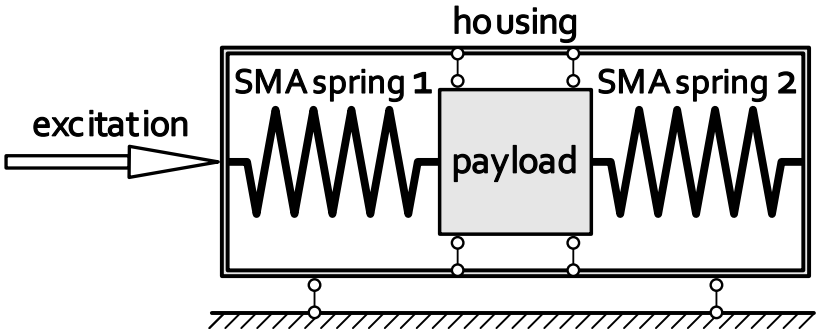

Fig. 1. Schematic diagram of the vibration protection device

The mechanical response of the springs is described by the microstructural model presented in the previous section with a set of material constants listed in Table 1. To analyze the device's behavior under various conditions, the initial phase state of the spring material (austenite or martensite) was determined by selecting a temperature. The modeling assumed that heat exchange between the springs and the surrounding medium occurs sufficiently rapidly, and that temperature changes due to heat generation and absorption during martensitic transformations can be neglected.

Table 1. Material constants for TiNi alloy

Material constant	Symbol	Value
Number of martensite variants	N	12
Latent heat (enthalpy) of the direct martensitic transformation, MJ/m^3	q_0	-180
Characteristic temperatures of martensite transformation, K	M_f M_s A_s A_f	303 323 340 360
Temperature of the thermodynamic equilibrium, K	T_0	341.5
Interaction coefficient of martensite variants	α	0.2
Microplastic strain scaling factor	κ	2.3
Coefficient of isotropic hardening, MPa	a_y	0.2
Coefficients of kinematic hardening, MPa	a_p	5
Maximum value of the oriented defects density	β^*	2.8
Initial value of scattered defects	f_0	20
Scattered defects recovery coefficient	r_1	0
Young's modulus of austenite, GPa	E_A	83
Young's modulus of martensite, GPa	E_M	41

The system is subjected to a harmonic vibration with a specified amplitude and frequency. The payload is assumed to move along one direction only, allowing this oscillatory system to be considered one-dimensional. The main geometric parameters of the springs and the characteristics of the system are given in Table 2.

Table 2. Characteristics of a vibration isolation device

Model Parameter	Symbol	Value
Wire diameter, mm	d_1, d_2	0.5
Coil diameter, mm	D_1, D_2	8.0
Number of coils	-	5
Mass of payload, kg	m	0.22
Drag coefficient	μ	0.5

The movement of the payload is described by the equation:

$$m\ddot{x} = -F_1 + F_2 - \mu\dot{x}, \quad (16)$$

where F_1 and F_2 are the elastic forces arising in the springs; μ is the drag coefficient (viscous friction).

Assuming that the wire experiences only torsion and the stress distribution is linear, we obtain:

$$F_1 = k_1\tau_1,\ F_2 = k_2\tau_2, \quad (17)$$

$$k_1 = \frac{\pi d_1^3}{8D_1},\ k_2 = \frac{\pi d_2^3}{8D_2}, \quad (18)$$

where τ_1, τ_2 are the shear stresses of the material, k_1 and k_2 are the spring stiffnesses, D_1 and D_2 are the diameters of coils, d_1 and d_2 are the wire diameters. Within the framework of the microstructural model, this differential equation is solved numerically using the improved Euler method.

Influence of microplastic deformation

Comparative analysis strategy

A key advantage of the microstructural model used is the ability to selectively account for individual deformation mechanisms. In this work, this allowed us to conduct a series of comparative calculations for two scenarios: one with and one without MPD. This approach allows us to quantitatively estimate the influence of this irreversible process on the damping characteristics and overall performance of the vibration isolation device. The calculations were performed for two initial phase states of the springs material: martensitic (at temperature of 300 K) and austenitic (at temperature of 380 K).

The choice of a temperature of 380 K for the austenitic state (which is 20 degrees higher than the end temperature of the reverse transformation A_f for the selected alloy) guarantees the full realization of the superelastic effect, as well as a temperature reserve necessary to compensate for the possible shift in characteristic temperatures (in particular, A_f) due to the accumulation of MPD. Without this reserve, MPD could lead to incomplete reverse transformation upon unloading and, consequently, to the degradation of the pseudoelastic hysteresis. A further increase in temperature is impractical, as it would shift the hysteresis toward higher stresses. In this case, over a wider stress range, the springs would have a linear-elastic behavior, rather than a pseudo-elastic one, which would lead to a decrease in the damping capacity, since the main contribution to this characteristic is made by the dissipation of energy during the phase transformation.

Determining resonance frequencies

Of greatest practical interest is the system's behavior in the resonant mode, which is the most challenging for any vibration isolation device. However, due to the significant nonlinearity of the SMA deformation properties caused by phase transformations, analytical determination of the resonant frequency is impossible. Therefore, for each of the studied cases (with and without MPD, for each phase state), the resonant frequency was determined numerically. The method involved performing a series of calculations varying the frequency of the external excitation and then identifying the frequency corresponding to the maximum amplitude of the payload mass oscillations.

The results of the numerical resonance identification procedure confirm the significant influence of microplasticity on the system's dynamic response. This is evident from the results presented in Fig. 2, which shows the dependence of the payload oscillation amplitude on the frequency of external excitation with an amplitude of 70 mm for springs in the martensitic state. The resonant frequencies, corresponding to the peak oscillation amplitudes marked by arrows, are distinctly different for the cases with and without accounting for microplasticity. This shift occurs because the accumulation of MPD alters the effective stiffness of the material. Consequently, to ensure a correct comparison of the damping capacity, the subsequent analysis of the system's performance is conducted at their respective resonant frequencies for each excitation amplitude.

The simulation results presented on Fig. 3 confirmed a characteristic feature of materials with nonlinear deformation dependencies: the resonant frequency of a vibration isolation system with SMA springs depends significantly on the amplitude of the external excitation.

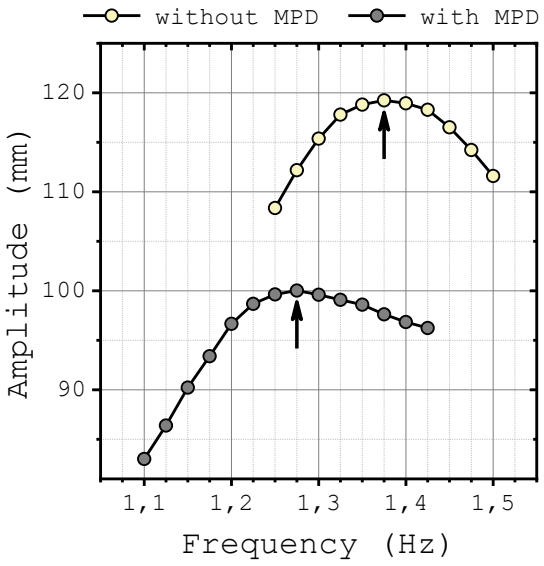

Fig. 2. Dependence of the amplitude of payload oscillation on the frequency of external excitation at a temperature of 300 K (martensite). The amplitude of external influence is 70 mm

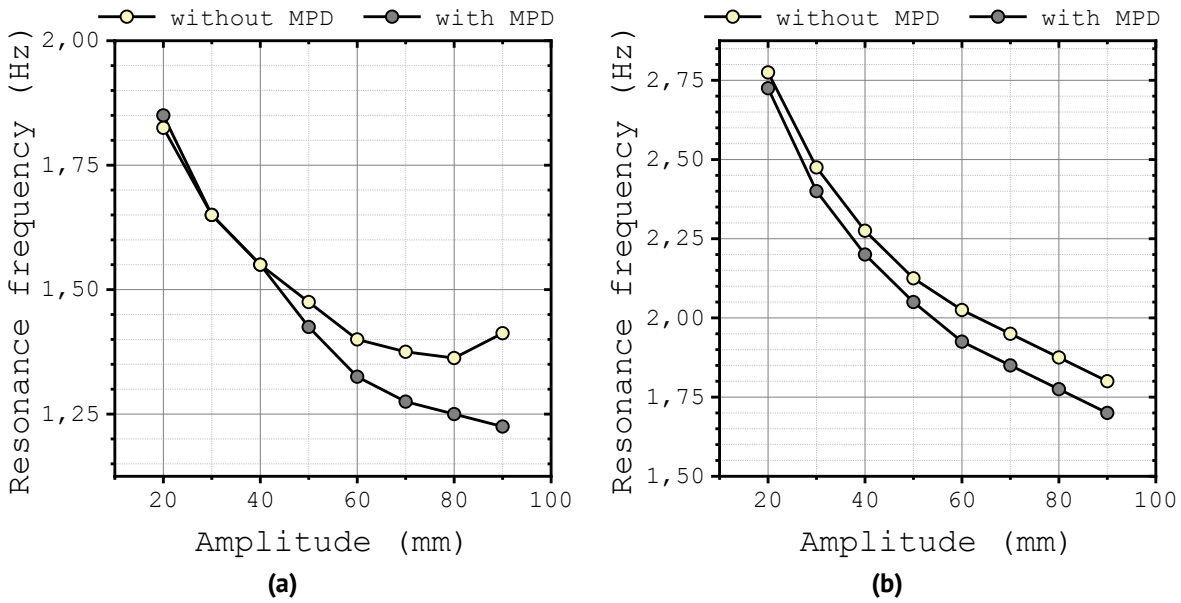

Fig. 3. Dependences of the resonance frequency on the amplitude of the external excitation in the martensitic state, at a temperature of 300 K (a) and in the austenitic state, at a temperature of 380 K (b)

It was found that for both initial phase states (austenitic and martensitic), taking MPD into account leads to a systematic decrease in the resonant frequency compared to the case where microplastic flow is not accounted (Fig. 3). This decrease is explained by the fact that microplasticity is an additional irreversible deformation mechanism that contributes to an increase in the overall deformation of the system and, consequently, a decrease in its effective stiffness.

Importantly, the difference between the resonant frequencies in simulations with and without accounting of microplastic flow increases with increasing excitation amplitude. This fact is consistent with the physics of the process: at high amplitudes and, correspondingly, high stresses, the intensity of microplastic flow increases, enhancing its

contribution to the overall mechanical response. In contrast, in the martensitic state, at excitation amplitudes of 40 mm or less, the dependences for both cases are almost identical (Fig. 3(a)). This is explained by the fact that the developed stresses are insufficient to activate MPD, and its influence can be neglected.

The influence of microplasticity on the deformation and force response of SMA springs

Analysis of the data presented in Figs. 4 and 5 reveals a significant influence of microplasticity on the response of the vibration isolation device. Accounting for MPD leads to a reduction in both the spring deformation amplitude and the maximum stresses in the material. This effect demonstrates a clear dependence on the loading level: the difference in deformations and stresses between the two cases increases significantly with increasing external excitation amplitude. For example, with an excitation amplitude of 90 mm, the calculated deformation values in the model accounting for MPD are more than two times lower.

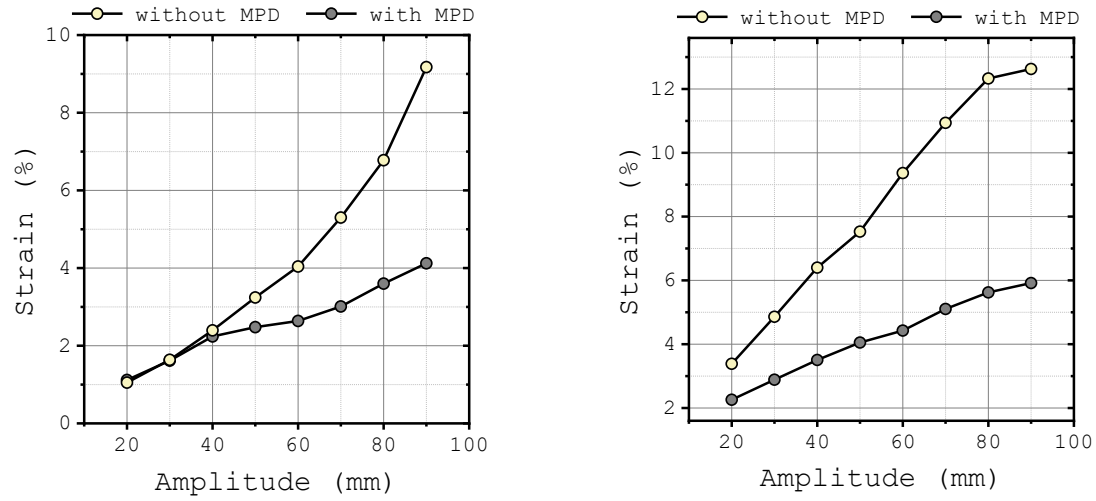

Fig. 4. Dependences of the strain amplitude on the amplitude of external excitation in the martensitic state (temperature of 300 K) (a) and in the austenitic state (temperature of 380 K) (b)

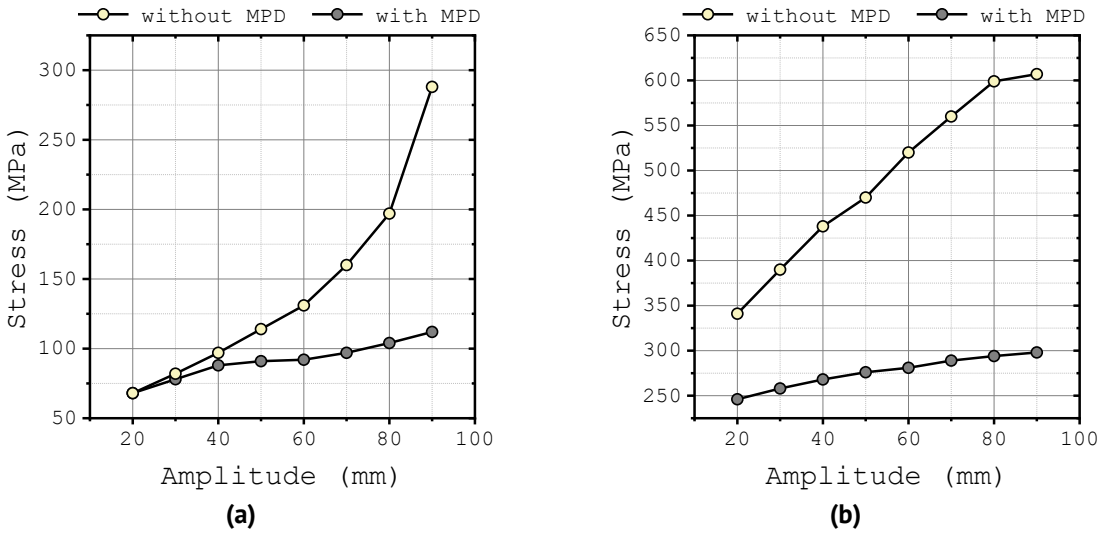

Fig. 5. Dependences of the stress amplitude on the amplitude of external excitation in the martensitic state (temperature of 300 K) (a) and in the austenitic state (temperature of 380 K) (b)

These results are explained by the fact that the energy expended on irreversible microplastic flow is diverted from the processes that determine elastic and phase deformation. As a result, the payload develops a smaller vibration amplitude, and lower stresses occur in the SMA springs. It's also worth noting that at small excitation amplitudes (up to 40 mm) in the martensitic state, the difference in strain and stress between the models becomes negligible (Figs. 4(a), 5(a)). This is consistent with previously obtained results — these amplitudes correspond to strains lying in the region of pure elasticity or elasticity with minor phase reorientation, which do not cause intense microplastic shear.

The obtained results demonstrate that when designing vibration protection devices operating in modes that lead to the occurrence of MPD, taking this mechanism into account is necessary for accurately predicting the dynamic characteristics of the system, in particular, its resonant frequency.

Evaluation of the effectiveness of SMA vibration protection devices

A key advantage of SMA-based vibration isolation devices over systems with conventional elastic elements is their ability to adapt to changing loading conditions, specifically, to avoid resonant modes due to the nonlinearity of their deformation characteristics.

In the austenitic state, nonlinearity is caused by direct martensitic transformation under load (pseudoelasticity). As Fig. 6 shows, with increasing deformation amplitude, the effective stiffness of the device, determined by the slope of the k_1 – k_3 lines for amplitudes of 2.5, 5, and 7.5 %, respectively, decreases significantly compared to the stiffness of a linear elastic element k_0 (with Young's modulus of austenite).

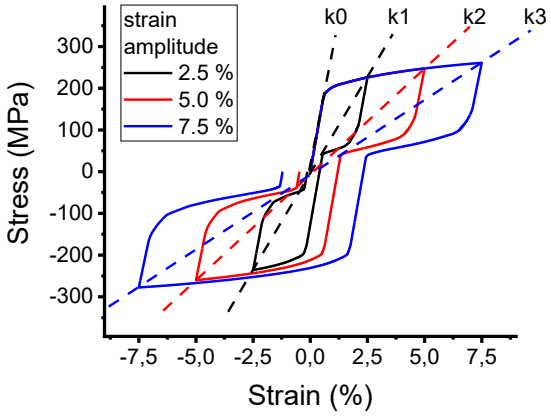

Fig. 6. Two-sided deformation of the TiNi alloy in the austenitic state (temperature of 380 K)

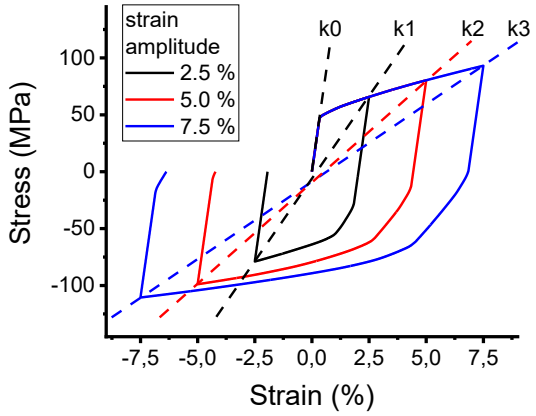

Fig. 7. Two-sided deformation of the TiNi alloy in the martensitic state (temperature of 300 K)

In the martensitic state, the nonlinear response arises from the reorientation of martensite variants. The two-way strain diagrams with amplitudes of 2.5, 5, and 7.5 %, shown in Fig. 7, are qualitatively similar to the strain curves of plastic materials. However, the fundamental difference is that deformation in the SMA is largely reversible. Analysis of the slopes of the secants k_1 – k_3 in the Fig. 7 also confirms a decrease in effective stiffness with increasing amplitude of deformation.

The identified nonlinearity forms a positive feedback loop that ensures system adaptation. If the frequency of the external excitation coincides with the natural frequency of the system, determined by the current effective stiffness, this leads to an increase in the oscillation amplitude. In a system with an elastic element, this would cause classical resonance. However, in a system with an SMA, increasing strain leads to a decrease in the effective stiffness, which, in turn, causes a change (decrease) in the system's natural frequency. As a result, the system "moves" away from the resonant frequency of the excitation, limiting the increase in oscillation amplitude.

To quantitatively evaluate the advantages of the SMA for the vibration isolation system under consideration, a comparative simulation of forced vibrations was conducted. Three configurations were studied: with SMA springs in the austenitic and martensitic states, and, for comparison, with conventional linear elastic springs. The stiffness of these reference elastic springs was set equal to the initial stiffness of the austenitic SMA spring (prior to any stress-induced phase transformation), thereby providing a direct baseline for comparison. The excitation was applied with an amplitude of 50 mm in a frequency range of 1 to 6 Hz.

The results, presented in Fig. 8, clearly demonstrate the superiority of SMA-based systems. The configuration with elastic elements exhibits a pronounced resonant peak with a sharp increase in the payload oscillation amplitude. Meanwhile, systems with SMA springs effectively suppress resonant phenomena, preventing a catastrophic increase in amplitude. Moreover, SMA springs in both austenitic and martensitic states, in almost the entire studied frequency range, show a higher efficiency of isolating the payload compared to a linear-elastic analogue.

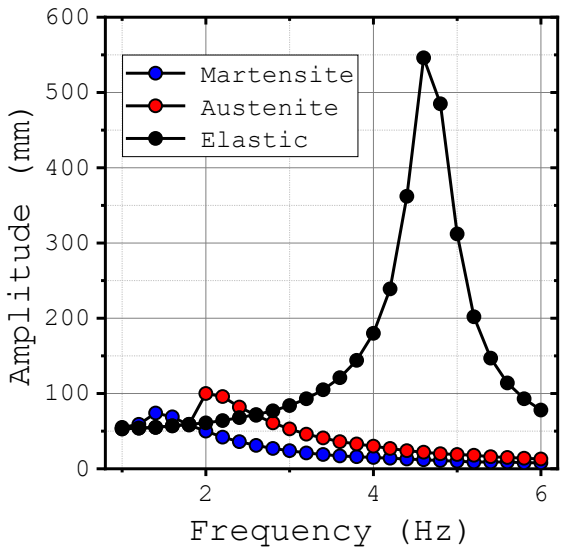

Fig. 8. Dependences of the amplitude of oscillations of the payload on the frequency of the excitation with an amplitude of 50 mm for springs in the martensitic (blue), austenitic (red) states and for the elastic element (black)

The conducted modeling allows for a comparative analysis of the effectiveness of SMA springs in various phase states. As Fig. 8 shows, in the frequency range above 2 Hz, the effective mass oscillation amplitude for springs in the martensitic state is

approximately half that of austenitic springs. This effect is explained by the lower effective stiffness and high damping in martensite, caused by the reorientation process.

Therefore, when designing vibration isolation devices, it should be taken into account that the martensitic state is preferable for active vibration damping applications, where the key goal is to minimize vibration amplitude. However, if the priority is maintaining the geometry and self-centering of the structure after strong disturbances, operation in the austenitic state is essential.

Conclusions

This study developed a model of a vibration isolation device based on a TiNi shape memory alloy springs. Using numerical simulation, a comparative analysis of the system's performance was performed with and without MPD. The following key results were obtained:

1. Accounting for microplasticity is critical for accurately predicting the resonant frequencies and damping characteristics of the device at significant loading amplitudes. It was shown that MPD leads to a systematic decrease in the resonant frequency and maximum spring deformations. The magnitude of this effect increases with increasing excitation amplitude.
2. A threshold effect of MPD was established. At low amplitudes (up to ~ 40 mm in the martensitic state), its contribution to the overall system response is negligible, and the device's behavior can be adequately described without taking this mechanism into account.
3. Comparative modeling demonstrated the significant advantage of SMA springs over linear elastic elements. SMA-based devices not only effectively suppress resonance but also reduce vibration amplitudes over a wide frequency range. It was found that the martensitic state provides maximum damping (the amplitudes are reduced by half compared to the austenitic state at frequencies above 2 Hz), while the austenitic state ensures self-centering of device.

Thus, the presented model, which takes MPD into account, enables highly accurate prediction of the behavior of SMA-based vibration protection devices over a wide range of operating conditions and serves as an effective tool for their design.

CRediT authorship contribution statement

Fedor S. Belyaev: conceptualization, investigation, writing – original draft; **Aleksandr E. Volkov**: writing – review & editing, supervision; **Margarita E. Evard**: writing – review & editing, supervision; **Maria S. Starodubova**: investigation.

Conflict of interest

The authors declare that they have no conflict of interest.

References

1. Mohd Jani J, Leary M, Subic A, Gibson MA. A review of shape memory alloy research, applications and opportunities. *Materials & Design (1980-2015).* 2014;56: 1078–1113.

2. Abul H, Safkat TA, Hafiz A. A review of utilizing shape memory alloy in structural safety. *AIUB Journal of Science and Engineering (AJSE).* 2020;19(3): 116–125.
3. Alam MS, Youssef MA, Nehdi M. Utilizing shape memory alloys to enhance the performance and safety of civil infrastructure: a review. *Canadian Journal of Civil Engineering.* 2007;34(9): 1075–1086.
4. Azarbayjani A, Edalat ME, Kheirikhah MM. Earthquake vibration control devices based on shape memory alloys: a review. In: *Proceedings of the 6th International Conference of Seismology and Earthquake Engineering, SEE6-2011, 16–18 May 2011, Tehran, Iran.* Tehran, Iran; 2011.
5. Humbeeck JV, Kustov S. Active and passive damping of noise and vibrations through shape memory alloys: applications and mechanisms. *Smart Materials and Structures.* 2005;14: S171–S185.
6. Kim S. Passive control techniques in earthquake engineering. In: Johnson CD. (Eds.) *Proceedings of the Smart Structures and Materials 1995: Passive Damping, 26 February – 3 March 1995, San Diego, United States.* San Diego, United States; 1995.
7. Buckle IG. Passive control of structures for seismic loads. *Bulletin of the New Zealand Society for Earthquake Engineering.* 2000;33(3): 209–221.
8. Jahangira H, Bagheri M. Evaluation of Seismic Response of Concrete Structures Reinforced by Shape Memory Alloys (Technical Note). *International Journal of Engineering. TRANSACTIONS C: Aspects.* 2020;33(3): 410–418.
9. McCormick J, DesRoches R, Fugazza D, Auricchio F. Seismic Vibration Control Using Superelastic Shape Memory Alloys. *Journal of Engineering Materials and Technology.* 2006;128(3): 294–301.
10. Menna C, Auricchio F, Asprone D. Chapter 13 - Applications of Shape Memory Alloys in Structural Engineering. In: Lecce L, Concilio A. (Eds.) *Shape Memory Alloy Engineering For Aerospace, Structural and Biomedical Applications.* Butterworth-Heinemann; 2015. p.369–403.
11. Somraj D, Surajit D, Purnachandra S. State of art review of shape memory alloy used in civil structures as seismic control device. *IJRET: International Journal of Research in Engineering and Technology.* 2015;04(13): 195–203.
12. Song G, Ma N, Lib HN. Applications of shape memory alloys in civil structures. *Engineering Structures.* 2006;28(9): 1266–1274.
13. Dolce M, Cardone D. Mechanical behaviour of shape memory alloys for seismic applications. Martensite and austenite NiTi bars subjected to torsion. *International Journal of Mechanical Sciences.* 2001;43(11): 2631–2656.
14. Cai W, Lu XL, Zhao LC. Damping behavior of TiNi-based shape memory alloys. *Materials Science and Engineering: A.* 2005;394(1–2): 78–82.
15. Haghdoust P, Conte AL, Cinquemani S, Lecis N. Experimental and Numerical Characterization of High Damping Martensitic CuAlMn Sheets. *Materials.* 2020;13(3): 529.
16. Saedi S, Acar E, Raji H, et al. Energy damping in shape memory alloys: A review. *Journal of Alloys and Compounds.* 2023;956: 170286.
17. Silwal B, Michael RJ, Ozbulut OE. A superelastic viscous damper for enhanced seismic performance of steel moment frames. *Engineering Structures.* 2015;105: 152–164.
18. Shinozuka M, Chaudhuri SR, Mishra SK. Shape-Memory-Alloy supplemented Lead Rubber Bearing (SMA-LRB) for seismic isolation. *Probabilistic Engineering Mechanics.* 2015;41: 34–45.
19. Qiu C, Zhu S. Shake table test and numerical study of self-centering steel frame with SMA braces. *Earthquake Engineering & Structural Dynamics.* 2017;46(1): 117–37.
20. Fang C, Yam MCH, Chan TM, Wang W, Yang X, Lin X. A study of hybrid self-centring connections equipped with shape memory alloy washers and bolts. *Engineering Structures.* 2018;164: 155–168.
21. Wang W, Fang C, Liu J. Self-Centering Beam-to-Column Connections with Combined Superelastic SMA Bolts and Steel Angles. *Journal of Structural Engineering.* 2017;143(2): 04016175.
22. Robertson SW, Pelton AR, Ritchie RO. Mechanical fatigue and fracture of Nitinol. *International Materials Reviews.* 2012;57(1): 1–37.
23. Mahtabi MJ, Shamsaei N, Mitchell MR. Fatigue of Nitinol: The state-of-the-art and ongoing challenges. *Journal of the Mechanical Behavior of Biomedical Materials.* 2015;50: 228–254.
24. Mahtabi MJ, Shamsaei N, Elahinia MH. Fatigue of Shape Memory Alloys. In: Elahinia MH. (Eds.) *Shape Memory Alloy Actuators: Design, Fabrication, and Experimental Evaluation.* John Wiley & Sons; 2015. p.155–190.
25. Tamai H, Kitagawa Y. Pseudoelastic behavior of shape memory alloy wire and its application to seismic resistance member for building. *Computational Materials Science.* 2002;25(1–2): 218–227.
26. Salehi M, Hodgson D, Parnell TK, DesRoches R, Mild E. Experimental evaluation of SMA-based multi-ring damping devices. *Smart Materials and Structures.* 2022;31(11): 115002.
27. Ding C, Wang B, Zhao J, Chen P, Ma K. Seismic resilient reinforced concrete structural wall system with distributed shape memory alloy U-shaped dampers. *Engineering Structures.* 2025;343(D): 121280.

28. Speicher M, Hodgson DE, DesRoches R, Leon RT. Shape Memory Alloy Tension/Compression Device for Seismic Retrofit of Buildings. *Journal of Materials Engineering and Performance.* 2009;18: 746–753.
29. Fang C, Wang W, Zhang A, Sause R, Ricles J, Chen Y. Behavior and Design of Self-Centering Energy Dissipative Devices Equipped with Superelastic SMA Ring Springs. *Journal of Structural Engineering.* 2019;145(10): 04019109.
30. Pappada S, Gren P, Tatar K, Gustafson T, Rametta R, Rossini E, Maffezzoli A. Mechanical and vibration characteristics of laminated composite plates embedding shape memory alloy superplastic wires. *Journal of Materials Engineering and Performance.* 2009;18: 531–564.
31. Zhang RX, Ni QQ, Mauda A, Yamamura T, Iwamoto M. Vibration characteristics of laminated composite plates with embedded shape memory alloys. *Composite Structures.* 2006;74: 389–398.
32. Kothalkar AD, Benitez R, Hu L, Radovic M, Karaman I. Thermo-mechanical response and damping behavior of shape memory alloy—MAX phase composites. *Metallurgical and Materials Transactions A.* 2014;45: 2646–2658.
33. Zhang XX, Hou HW, Wei LS, Chen ZX, Wei WT, Geng L. High damping capacity in porous NiTi alloy with bimodal pore architecture. *Journal of Alloys and Compounds.* 2013;550: 297–301.
34. Huang H, Mosalam KM, Chang W. Adaptive tuned mass damper with shape memory alloy for seismic application. *Engineering Structures.* 2020;223: 111171.
35. Rustighi E, Brennan MJ, Mace BR. A shape memory alloy adaptive tuned vibration absorber: design and implementation. *Smart Materials and Structures.* 2005;14(1): 19.
36. Parlinska M, Balta JA, Michaud V, Bidaux JE, Månson JA, Gotthardt R. Vibrational response of adaptive composites. *Journal de Physique IV.* 2001;11(PR8): 129–134.
37. Parlinska M, Clech H, Balta JA, Michaud V, Bidaux JE, Manson JAE, Gotthardt R. Adaptive composites with embedded shape memory alloys. *Journal de Physique IV.* 2001;11(PR): 197–204.
38. Moradi S, Nia MM. Developing Predictive Equations for the Self-Centering Response of Beam-Column Connections with Steel Angles and Shape Memory Alloy Bolts. In: Gupta R, Sun M, Brzev S, Alam MSh, Ng KTW, Li J, El Damatty A, Lim C. (Eds.) *Proceedings of the Canadian Society of Civil Engineering Annual Conference 2022.* Cham: Springer; 2024. p.1253–1264.
39. Parulekar YM, Reddy GR. Nonlinear Model of Pseudoelastic Shape Memory Alloy Damper Considering Residual Martensite Strain Effect. *Advances in Acoustics and Vibration.* 2012;2012: 261896.
40. Volkov AE, Evard ME, Vikulenkov AV, Uspenskiy ES. Simulation of Vibration Isolation by Shape Memory Alloy Springs Using a Microstructural Model of Shape Memory Alloy. *Materials Science Forum.* 2013;738–739: 150–154.
41. Volkov AE, Evard ME, Red'kina KV, Vikulenkov AV, Makarov VP, Moisheev AA, Markachev NA, Uspenskiy ES. Simulation of Payload Vibration Protection by Shape Memory Alloy Parts. *Journal of Materials Engineering and Performance.* 2014;23: 2719–2726.
42. Evard ME, Volkov AE. Modeling of Martensite Accommodation Effect on Mechanical Behaviour of Shape Memory Alloys. *Journal of Engineering Materials and Technology.* 1999;121(1): 102–104.
43. Simon T, Kröger A, Somsen C, Dlouhy A, Eggeler G. On the multiplication of dislocations during martensitic transformations in NiTi shape memory alloys. *Acta Materialia.* 2010;58(5): 1850–1860.
44. Sidharth R, Mohammed ASK, Sehitoglu H. Functional Fatigue of NiTi Shape Memory Alloy: Effect of Loading Frequency and Source of Residual Strains. *Shape Memory and Superelasticity.* 2022;8: 394–412.
45. Belyaev FS, Volkov AE, Evard ME. Microstructural modeling of fatigue fracture of shape memory alloys at thermomechanical cyclic loading. *AIP Conference Proceedings.* 2018;1959(1): 070003.
46. Belyaev FS, Evard ME, Volkov AE. Simulation of the plastic deformation of shape memory alloys considering shear anisotropy on the slip plane. *Materials Physics and Mechanics.* 2023;51(1): 61–67.
47. Resnina NN, Ivanov AM, Belyaev FS, Volkov AE, Belyaev SP. Simulation of recoverable strain variation during isothermal holding of the Ni51Ti49 alloy under various regimes. *Letters on Materials.* 2023;13(1): 33–38.
48. Volkov AE, Belyaev FS, Volkova NA, Vukolov EA, Evard ME, Rebrov TV. The effect of martensite stabilization in titanium nickelide after various methods of pre-deformation: simulation with a single set of constants. *Materials Physics and Mechanics.* 2024;52(4): 91–99.
49. Belyaev FS, Volkov AE, Vukolov EA, Evard ME, Kudrina KV, Starodubova MS. Influence of latent heat and heat exchange conditions on tension behavior of shape memory alloy specimen. *Materials Physics and Mechanics.* 2024;52(5): 18–28.
50. Belyaev FS, Volkov AE, Gorbachenko DF, Evard ME. Modeling of working cycles of thermomechanical actuators based on shape memory alloys at repeated actuation. *Materials Physics and Mechanics.* 2024;52(6): 81–90.
51. Belyaev FS, Volkov AE, Evard ME, Volkova NA. A Microstructural model of SMA with Microplastic Deformation and Defects Accumulation: Application to Thermocyclic Loading. *Materials Today: Proceedings.* 2015;2(3): S583–S587.
52. Volkov AE, Belyaev FS, Evard ME, Volkova NA. Model of the Evolution of Deformation Defects and Irreversible Strain at Thermal Cycling of Stressed TiNi Alloy Specimen. *MATEC Web of Conferences.* 2015;33: 03013.